Metabolic Reconstruction and Modeling Microbial Electrosynthesis

Christopher W. Marshall[1,3]*, Daniel E. Ross[7], Kim M. Handley[4#], Pamela B. Weisenhorn[1], Janaka N. Edirisinghe[4], Christopher S. Henry[4], Jack A. Gilbert[1,3], Harold D. May[5,6], and R. Sean Norman[7]*

1. Biosciences Division, Argonne National Laboratory, Argonne, Illinois, USA;
2. Department of Ecology and Evolution, The University of Chicago, Chicago, Illinois, USA;
3. Department of Surgery, The University of Chicago, Chicago, Illinois, USA;
4. Computing, Environment, and Life Sciences, Argonne National Laboratory, Illinois, USA;
5. Department of Microbiology and Immunology, Medical University of South Carolina, Charleston, South Carolina, USA;
6. Marine Biomedicine and Environmental Science Center, Medical University of South Carolina, Charleston, South Carolina, USA;
7. Department of Environmental Health Sciences, Arnold School of Public Health, University of South Carolina, Columbia, South Carolina, USA;

#Present address: Kim M. Handley, School of Biological Sciences, The University of Auckland, Auckland, New Zealand.
*Corresponding authors
Correspondence: CW Marshall, Department of Surgery (Room O-200C, MC 5030), University of Chicago, 5841 S Maryland Ave., Chicago, IL 60637. E-mail: chris.w.marshall@gmail.com. RS Norman, Department of Environmental Health Sciences, University of South Carolina, 931 Assembly St., Columbia, SC 29208. E-mail: rsnorman@sc.edu

Running title: Modeling a Microbial Electrosynthetic Community

Abstract

Microbial electrosynthesis is a renewable energy and chemical production platform that relies on microbial taxa to capture electrons from a cathode and fix carbon. Yet the metabolic capacity of multispecies microbial communities on electrosynthetic biocathodes remains unknown. We assembled 13 genomes from a high-performing electroacetogenic culture, and mapped their transcriptional activity from a range of conditions. This allowed us to create a metabolic model of the primary community members (*Acetobacterium*, *Sulfurospirillum,* and *Desulfovibrio*). *Acetobacterium* was the primary carbon fixer, and a keystone member of the community. Based on transcripts upregulated near the electrode surface, soluble hydrogenases and ferredoxins from *Acetobacterium* and hydrogenases, formate dehydrogenase, and cytochromes of *Desulfovibrio* were essential conduits for electron flow from the electrode into the electrosynthetic community. A nitrogenase gene cluster with an adjacent ferredoxin and one of two Rnf complexes within the genome of the *Acetobacterium* were also upregulated on the electrode. Nitrogenase is known to serve as a hydrogenase, thereby it would contribute to hydrogen production by the biocathode. Oxygenases of microaerobic members of the community throughout the cathode chamber, including *Sulfurospirillum* and *Rhodobacteraceae,* were expressed. While the reactors were maintained anaerobically, this gene expression would support anaerobic growth and thus electrosynthesis by scrubbing small amounts of O_2 out of the reactor. These

molecular discoveries and metabolic modeling now serve as a foundation for future examination and development of electrosynthetic microbial communities.

Introduction

A microbial electrosynthesis system (MES) is a bioelectrochemical device that employs microbes to transport electrons from a cathode to protons and/or CO_2. Thus, the microbes act as cathode catalysts to generate, or synthesize, a valuable product (Rabaey and Rozendal, 2010). This technology has immense potential, therefore understanding which microbes are capable of cathodic electron transfer and which metabolic pathways are involved in CO_2 conversion to chemicals are critical to improving the performance of MESs. Furthermore, this work has broader environmental implications including understanding ecological aspects of one carbon metabolism and extracellular electron transfer relevant to global biogeochemical cycling. Technologically, these MESs could have a significant impact on geoengineering applications such as carbon capture and storage.

Advances in microbial electrosynthesis and related biocathode-driven processes primarily focus on the production of three compounds: hydrogen (electrohydrogenesis)(Rozendal *et al.*, 2008), methane (electromethanogenesis) (Cheng *et al.*, 2009), and acetate (electroacetogenesis) (Nevin *et al.*, 2010). However, microbial electrosynthesis can be used to generate alcohols and various short-chain fatty acids.\ (Steinbusch *et al.*, 2010). A thorough evaluation of a carbon dioxide fixing aerobic biocathode has also been reported (Wang *et al.*, 2015). To manipulate (and optimize) these systems we must understand the extracellular electron transfer (EET) enzymes or molecules involved in cathode oxidation, and we must determine how these cathodic electron transport components are coupled to energy conservation by the microbial cell. While an increasingly robust body of literature has been established relating to microbial

communities metabolizing with an anodic electron acceptor (Ishii *et al.*, 2013, 2015; Kiely *et al.*, 2011), much is still unclear about the diverse metabolic capabilities of microorganisms and communities growing on a cathode (Tremblay and Zhang, 2015). We used metagenomics, metatranscriptomics, and metabolic flux modeling to elucidate carbon flux and EET mechanisms. We have deciphered the complex interactions between cooperating and competing members of the microbiome, producing opportunities to improve microbial electrosynthesis as well as understand multi-species biofilm communities.

Materials and Methods

Reactor design and operation

The reactors containing the microbial communities used for metagenomics and metatranscriptomics in this study were described in detail in two previous studies (Marshall *et al.*, 2012, 2013). Of the five MES reactors previously described, two reactors were selected for further analysis in this study. The first reactor, closed circuit (CC), was operated for 184 days before termination (MES-BW4 from previous manuscript is CC reactor here). The second reactor, open circuit (OC), was operated in closed circuit mode for 141 days before it was left at open circuit for three hours prior to termination, in order to control for biofilm effects of the closed circuit reactor (MES 1a from previous manuscript is OC reactor. The initial source of microorganisms was from a brewery wastewater retention basin that was then subjected to sequential transfers of the graphite and supernatant in bioelectrochemical systems before inoculation into the two MESs described in this study. The brewery wastewater inoculum was allowed to establish on graphite granule cathodes and then repeatedly washed with fresh defined medium containing per liter: 2.5 g $NaHCO_3$, 0.6 g NaH_2PO_4 * H_2O, 0.25 g NH_4Cl, 0.212 g $MgCl_2$, 0.1 g KCl, 0.03 g $CaCl_2$, 20 mL vitamin solution, and 20 mL mineral solution.

Subsequent, sludge-free transfers were made into 150 mL volume cathode chambers of MESs containing 30 g of graphite granules, 75 mL of medium, 80% N_2 and 20% CO_2 or 100% CO_2 in the headspace, and poised at -590 mV vs. standard hydrogen electrode (SHE) for the duration of the experiments unless otherwise noted. The medium during the initial startup period did not contain sodium 2-bromoethanesulfonate (2-BES), but 10 mM 2-BES was periodically used to inhibit methanogenesis and maintain a predominantly acetogenic culture later in the study, including at the time of sampling for metagenome and metatranscriptome analyses (day 181). Upon termination of the experiment, supernatant and bulk granular cathodes were removed for DNA and RNA extraction. All samples were frozen in liquid nitrogen within 5 minutes of applied voltage interruption, except OC which was deliberately left at open circuit for 3 hours prior to freezing. A schematic of the experimental design can be found in Supplementary Figure 1.

DNA/RNA extraction and sequencing

DNA and RNA were processed as previously reported and is detailed in the Supplementary Online Methods. Whole genome shotgun sequencing of the cathode-associated microbial community from the closed circuit reactor (CCc) and the supernatant community from the closed circuit reactor (CCs) was accomplished with the Illumina MiSeq instrument yielding 250 bp paired-end reads totaling 9,793,154 reads with a total length of 2,325,061,111 bp for the attached microbial community, and 5,049,632 reads with a total length of 1,198,063,143 bp for the supernatant microbiome.

Metagenome assembly and binning

Two metagenomes were assembled and annotated from the closed circuit reactor (CCc and CCs). Near full-length 16S rRNA sequences from the CCc and CCs metagenomes were assembled over 100 iterations of the Expectation-Maximization Iterative Reconstruction of Genes from the Environment (EMIRGE) method (Miller *et al.*, 2011), following initial read mapping to a modified version of the dereplicated version of the SILVA 108 small-subunit (SSU) rRNA database (Quast *et al.*, 2013). During iterations sequences 97% similar were clustered. Representative sequences were searched against the SSURef_111_NR_trunc database using BLASTN.

SPAdes (Bankevich *et al.*, 2012), Velvet+Metavelvet (Zerbino and Birney, 2008; Namiki *et al.*, 2012), Ray (Boisvert *et al.*, 2012), and IDBA-UD (Peng *et al.*, 2012) community genome assemblies were compared based on total length of the assembly, n50 score, and percent reads mapping back to the assemblies (Supplementary Table 1). Based on the assembly results, the SPAdes assembly was used to further analyze the metagenomes due to the highest percent of reads mapped to a threshold above 1kb (cathode: 95.95%, supernatant: 91.61%) and total assembly size (cathode: 67,511,580 bp above 1kb, supernatant: 42,119,276 bp). Following assembly, the SPAdes contigs were analyzed by Prodigal (Hyatt *et al.*, 2010) to predict protein-encoding genes. Prodigal-predicted amino acid sequences were then annotated using UBLAST searches (usearch64(Edgar, 2010)) against the uniref90 database (Suzek *et al.*, 2015) with an e-value cutoff of 100. These annotations, along with kmer coverage and GC content were used for preliminary genome binning. Emergent self-organizing maps (ESOM) were used to refine the metagenome bins based on tetranucleotide frequency and contig coverage on contigs greater than 4kb (Dick *et al.*, 2009). Smaller fragments (>1kb) were then projected onto the 4kb ESOM. To further refine the bins the multi-metagenome pipeline (Albertsen *et al.*, 2013) was used, leveraging differential genome coverages

between CCc and CCs to aid contig identification. Results were compared to ESOM bins. Only contigs binned by both ESOM and multi-metagenome pipeline were used for reassemblies of individual genome bins. All reads associated with the contigs in each of the final bins were reassembled as single organism genomes by SPAdes using default options with the addition of the –careful flag and kmer sizes of 65, 77, 99, and 127. All contigs greater than 1kb were uploaded to RAST (Aziz *et al.*, 2008) for final annotation using RASTtk (Brettin *et al.*, 2015). The re-assembled individual genome bins and one large "undetermined" bin were compiled into a combined metagenome for transcript mapping. See Supplementary Table 2 for bin summaries and completeness generated by CheckM (Parks *et al.*, 2015). The RASTtk annotations were compared to annotations (Wu *et al.*, 2011) from Pfam, COG, and a Blastx search of the non-redundant protein sequences database (Camacho *et al.*, 2009). The RAST-annotated protein encoding gene (peg) tags are used as identifiers throughout the manuscript with the bin abbreviation preceding the peg number. See Supplementary Table 3 for all annotations.

Metatranscriptome

Four total metatranscriptomes were recovered from CCc, CCs, OCc, and OCs. The FASTX toolkit was used to filter the reads with a quality score lower than 30 and a length less than 50bp. Quality filtered reads from each sample were mapped to the CCc electrode metagenome contigs using BWA (Li and Durbin, 2009). Raw hit counts mapped to each RAST-annotated protein encoding gene in the combined metagenome were then used to calculate reads per kilobase gene length per millions of mapped reads (RPKM) values. RPKM values for each gene were also normalized to bin coverage based on single copy *recA* gene abundances (Supplementary Figure 6). This compensated for the abundance variations of the taxa between samples. Quantile normalization was used to evenly distribute the transcript values between sample

conditions. Fold change for differential expression analysis between conditions was calculated by dividing RPKM/RecA-condition1 by RPKM/RecA-condition2. To eliminate 0 value errors and over interpretation of very low count genes, an empirically determined threshold value of 0.1 was added to all of the RPKM/RecA values.

Metabolic model reconstruction, gapfilling, and curation

To construct models of our three highest relative abundance genomes (*Acetobacterium*, *Sulfurospirillum*, and *Desulfovibrio*), we imported the RAST-annotated versions of these genomes into the DOE Systems Biology Knowledgebase (KBase). Once in KBase, we used the *Build Metabolic Model* app, which is based on the ModelSEED algorithm (Henry *et al.*, 2010), to construct one draft model for each genome. Once the draft models were complete, we curated the models based on literature data, KEGG (Kanehisa and Goto, 2000), and MetaCyc (Karp *et al.*, 2002)(Supplementary table 4c). This curation primarily involved the addition of electron utilization pathways (*Acetobacterium*), addition of electron transport chain reactions (*Sulfurospirillum*, and *Desulfovibrio*), and adjustment of reaction directionality to prevent pathways from proceeding in unphysiological directions.

Next, we applied the *Gapfill metabolic model* KBase app to identify and fill all the gaps in the metabolic pathways of our models that might prevent them from producing biomass while operating in one of our hypothesized metabolic roles within the microbial community. In this gap-filling process, the model was augmented to include all the reactions contained in the ModelSEED database (available for download from GitHub (https://github.com/ModelSEED/ModelSEEDDatabase/tree/master/Biochemistry). Additionally, all reactions determined to be thermodynamically reversible (Henry *et al.*, 2006, 2009; Jankowski *et al.*, 2008) were adjusted to be reversible. Finally, flux balance

207 analysis (FBA) (Orth *et al.*, 2010) was performed to generate a flux profile that produced
208 biomass while minimizing the flux through all reactions and reaction directions that were
209 not contained in the original model, consistent with previously published algorithms
210 (Dreyfuss *et al.*, 2013; Latendresse, 2014). All reactions and reaction directions not
211 included in the original model that had a nonzero flux in were then added to the model
212 as the gap-filling solution. This subsequently permits the growth of the gap-filled model
213 in the specified condition. *Acetobacterium* was gapfilled in a condition that reflected the
214 only proposed metabolic role for this organism: direct consumption of electrons to fix
215 CO2 coupled to the production of acetate. The *Sulfurospirillum* and *Desulfovibrio* models
216 were gapfilled separately in two distinct conditions reflecting the potential roles proposed
217 for these organisms: (i) autotrophic growth on CO_2 and H_2; or (ii) heterotrophic growth on
218 acetate. This produced a total of four models: (i) autotrophic *Sulfurospirillum*; (ii)
219 heterotrophic *Sulfurospirillum*; (iii) autotrophic *Desulfovibrio*; and (iv) heterotrophic
220 *Desulfovibrio*. The detailed composition of the electrosynthetic, autotrophic, and
221 heterotrophic media formulations used in the gapfilling analysis are included in the
222 supplementary material (Supplementary Table 4).
223
224 All models were reconstructed, gapfilled, and curated in the KBase Narrative Interface,
225 and the associated narratives include all parameters and media formulations used
226 (https://narrative.kbase.us/narrative/ws.15248.obj.1). All model data is also available for
227 download from the same narratives. The reactions for each model and condition can
228 also be found in Supplementary Table 4a.
229
230 **Prediction of metabolic activity with comparison to expression data**
231 Flux balance analysis (FBA) was applied with each of our gapfilled metabolic models to
232 simulate the production of biomass on the same media formulations used in our

gapfilling analysis (electrosynthetic, autotrophic, and heterotrophic media). Thus, we simulated the growth of our gapfilled *Acetobacterium* model in our electrosynthetic media; we simulated the growth of our autotrophic *Sulfurospirillum* and *Desulfovibrio* models in our autotrophic media; and we simulated the growth of our heterotrophic *Sulfurospirillum* and *Desulfovibrio* models in our heterotrophic media (all media formulations are listed in Supplementary table 4b). We then maximized the production of biomass in each model, subject to the constraints on nutrient uptake imposed by our media formulations, and once a solution was produced, we minimized the sum of the fluxes comprising the solution, in order to produce a single solution that is both simple and distinct.

We validated our flux solutions by comparing the active reactions in each flux profile against the actively expressed genes identified based on our transcriptomic data. In order to conduct this comparison, we first needed to classify the genes in our three species as either *active* or *inactive* based on the relative abundance of mapped RNA-seq reads. This process began by identifying an initial set of universal genes in each species that can be assumed to be *always active* (e.g. DNA polymerase subunits and tRNA synthetases). These genes are listed in Supplemental table 4d. We ranked these *always active* genes based on the abundance of reads mapped to them, identifying the number of reads mapped to the gene ranked at the 10^{th} percentile in this list as the threshold expression value. Then in the broader genome, we labeled any gene with mapped reads that exceeded the threshold as active, with all other genes being inactive. Finally, we calculated the binary distance between the transcriptome and flux profiles, excluding any reactions that had been gapfilled, to determine which predicted flux profiles yielded the greatest agreement (i.e. lower binary distance) with the transcriptomic data.

We carried out a comparative model analysis on thirty-three KEGG pathway categories involving gene presence and absence, transcriptomic data from CCc, flux analysis, and gap-filled reactions on each pathway category (Figure 3). Carbon fixation pathway categories (i.e. reductive TCA cycle and Wood- Ljungdahl pathways) were lumped into a single category called CO_2 fixation. All of the metabolic models, their associated genomes, and the FBA analysis generated in this study are presented using the KBase Narrative Interface (NI) and are accessible at https://narrative.kbase.us/narrative/ws.15248.obj.1.

Scanning electron microscopy - energy dispersive x-ray spectroscopy (SEM-EDX)

Cathodic graphite granules were fixed in 0.1 M sodium cacodylate buffer with 2% gluteraldehyde for three hours, washed in 2.5% osmium tetroxide, and then dehydrated with an ethanol dilution series using 0%, 25%, 50%, 75%, % and 100%. Samples were stored in a desiccator and then coated with Au and Pd using a Denton Vacuum sputter coater. Images were generated using a FEI Quanta 400 Scanning Electron Microscope.

Data access

The metagenomic and metatranscriptome reads can be found in MG-RAST (Meyer *et al.*, 2008) under the ID numbers (and names) 4673464.3-4673467.3 (ARPA_metagenome) for the metagenome (http://metagenomics.anl.gov/linkin.cgi?project=15936) and 4536830.3-4536839.3 (ARPA_metatranscriptome) for the metatranscriptomes (http://metagenomics.anl.gov/linkin.cgi?project=6065). Assembled contigs for *Acetobacterium, Sulfurospirillum,* and *Desulfovibrio* can be accessed at

https://narrative.kbase.us/narrative/ws.15248.obj.1. Raw Illumina sequencing reads have been deposited in the NCBI SRA database under Bioproject PRJNA245339. Additionally, sequencing and assembly files can be found online at https://github.com/sirmicrobe/electrosynthesis.

Results

Performance and compositions of microbial electrosynthesis systems

Two high performing MESs inoculated from an established electrosynthetic community were poised at -590 mV vs. a standard hydrogen electrode (SHE), and operated for over 100 days, generating an average percentage of total products formed of 65% acetate, 34% hydrogen, 0.4% formate, 0.3% propionate and 0.2% butyrate from CO_2. At the conclusion of the experiment, one of the two reactors was left at open circuit for three hours to distinguish between transcripts influenced by the supply of electrons from the cathode compared to electrons supplied by hydrogen and/or other free metabolites in the biofilm. Similarly, metatranscriptome samples were taken from the electrode surface and compared to the supernatant. This led to four metatranscriptome samples from two reactors: closed circuit cathode (CCc), closed circuit supernatant (CCs), open circuit cathode (OCc), and open circuit supernatant (OCs). Coulombic efficiencies at time of sampling were 77% and 73% from CC and OC, respectively (Figure 1). Thirteen genome bins spanning 5 different phyla were recovered from the assembled metagenomes taken from the closed circuit MES (Figure 2). Near-complete genomes (89-100% complete) were produced for *Sulfurospirillum* str. MES7, *Acetobacterium* str. MES1, *Desulfovibrio* str. MES5, *Methanobacterium* str. MES13, *Bacteroides* str. MES9, *Geobacter* str. MES3, and *Sphaerochaeta* str. MES8 (Supplementary Table 2), and a second partially complete (~65%) *Desulfovibrio* str. MES6 genome was further obtained. *Acetobacterium*, *Sulfurospirillum,* and *Desulfovibrio* combined comprised 40-90% of the

311 community in each condition, with a Rhodobacteraceae related organism also
312 consistently represented (4-20% relative abundance) (Figure 2, Supplementary Figure
313 2). The 13 annotated genome bins recovered from the CC reactor were used as the
314 basis for transcript mapping and analyses.
315
316 **Description of the microbial catalysts**
317 Three species, *Acetobacterium* str. MES1, *Sulfurospirillum* str. MES7, *Desulfovibrio* str.
318 MES5, comprised 72% of the total abundance on the active cathode (CCc). The
319 abundance, expression levels, and predominant activity in the reactor (acetogenesis) as
320 well as the known physiology of similar organisms indicates that the *Acetobacterium*
321 species is the main proponent of carbon fixation on the electrode and thus the keystone
322 species in the microbial community. Genomic and transcriptomic evidence indicates the
323 reconstructed *Acetobacterium* str. MES1 reduces CO_2 to acetate through the Wood-
324 Ljungdahl pathway (WLP). WLP-indicative acetyl-CoA synthase/carbon monoxide
325 dehydrogenase (ACS/CODH, aceto.peg.1971-1981) and 5-
326 methyltetrahydrofolate:corrinoid iron-sulfur protein methyltransferase (aceto.peg.1978)
327 components were among the most highly expressed genes on the closed circuit
328 electrode surface (Figure 3). Furthermore, the canonical enzyme ACS/CODH had on
329 average >3-fold greater expression on the closed circuit electrode compared to the
330 supernatant as well as higher expression on CCc compared to OCc, indicating that the
331 electrode surface was the major source of acetate production. Interestingly, a
332 *Clostridium*-type chain elongation pathway(Bruant *et al.*, 2010) was expressed in the
333 *Acetobacterium* str. MES1 to convert acetyl-CoA to butyrate (aceto.peg.1850-4, 2312),
334 which may explain the butyrate production by the electrosynthetic microbiome
335 (Supplementary Figure 3)(Marshall *et al.*, 2013).
336

Reducing equivalents for the Wood-Ljungdahl pathway, reduced ferredoxin and NADH, were generated by a soluble uptake hydrogenase complex, *hydABCDE* (aceto.peg.4025-9), which were the most highly expressed *Acetobacterium* str. MES1-associated hydrogenase genes on the electrode. The high expression of *hydABCDE* and *rnfABCDEG* gene clusters, suggests *Acetobacterium* str. MES1 conserves energy similar to *A. woodii.*(Schuchmann and Müller, 2014) The exception is that MES1 has two Rnf complex copies, one with 15-fold greater gene expression on the electrode surface (high: aceto.peg.2709-14 and low: aceto.peg.926-931). This expression difference is similar to *Azotobacter vinelandii* whose copy expression disparity is driven by ammonium depletion.(Curatti *et al.*, 2005) Rnf expression positively correlates with nitrogen fixation (*nif*) gene expression, which is likely because Rnf is required for stable accumulation of the 4Fe4S clusters in *nifH.*(Jeong and Jouanneau, 2000; Curatti *et al.*, 2005) *Acetobacterium* str. MES1 maintains a nitrogenase gene cluster (*nifBEHN*) (aceto.peg.248-54) with an adjacent ferredoxin. In fact *nifH* was in the top 5 most expressed *Acetobacterium* str. MES1 genes in all conditions, suggesting N-limitation and/or an involvement in electron transfer (Figure 3). As ammonium is depleted, nitrogenase converts protons to hydrogen in the absence of N_2 (Ryu *et al.*, 2014), which may contribute to the measured hydrogenesis. This supports previous observations of a lag time between fresh media exchange and the onset of hydrogenesis, and of a positive correlation between *Acetobacterium* and hydrogen production (LaBelle *et al.*, 2014). It is also possible that electron transfer from the Rnf complex to the nitrogenase for proton reduction is a source of hydrogen production by the electrosynthetic microbiome in this and related studies (LaBelle *et al.*, 2014), and is a potential target for biotechnological exploitation (Ryu *et al.*, 2014).

362 *Sulfurospirillum* str. MES7 remained consistently abundant (>60% relative abundance) in
363 the supernatant despite frequent exchanges with fresh medium. However, the role of
364 *Sulfurospirillum* in electrosynthesis has remained elusive (Marshall *et al.*, 2012, 2013).
365 Given its prevalence it must fix CO_2 and/or utilize acetate as a carbon source. In support
366 of CO_2 fixation, *Sulfurospirillum* spp. are hypothesized to fix CO_2(Goris *et al.*, 2014) and
367 other members of the epsilonproteobacteria can fix CO_2 via the reductive tricarboxylic
368 acid (rTCA) cycle (Hügler *et al.*, 2005). As shown here and a recent *Sulfurospirillum*
369 comparative genomic study (Ross *et al.*, 2016), the *Sulfurospirillum* str. MES7 assembly
370 contains several genes necessary to overcome the irreversible enzymes of the TCA
371 cycle, including a 2-oxoglutarate oxidoreductase alpha, beta, delta, and gamma subunits
372 (EC 1.2.7.3, sulfuro.peg.1237-40) and fumarate reductase (EC 1.3.5.1, sulfuro.peg.592-
373 4). No ATP citrate lyase or citryl-CoA lyase were found, but it does have genes for the
374 conversion of citrate to oxaloacetate + acetate (citrate lyase alpha and beta chains, and
375 citrate (pro-3S)-lyase, EC 4.1.3.6, sulfuro.peg.2133-6), suggesting the possibility of CO_2
376 fixation through rTCA. This is also supported by the transcriptional activity of key genes
377 in the rTCA cycle (Supplementary Figure 4). In addition, acetate permease
378 (sulfuro.peg.1580) and acetate kinase (sulfuro.peg.1274) are both highly expressed,
379 indicating either that a supplementary organic carbon source might be required for
380 growth, or that *Sulfurospirillum* str. MES7 flexibly switches between CO_2 fixation and
381 acetate oxidation in the MES reactor.
382
383 By far the most highly expressed genes relating to terminal electron accepting processes
384 in *Sulfurospirillum* str. MES7 (for any condition) were cytochromes, particularly
385 cytochrome c oxidases. C-type heme-copper oxidases are the final step in the catalytic
386 reduction of oxygen in certain bacteria (Lee *et al.*, 2011) and *ccoNOPQ* is highly
387 expressed by *Sulfurospirillum* str. MES7 (sulfuro.peg.1785-8) in all MES conditions. The

388 high expression of *ccoNOPQ* suggests *Sulfurospirillum* str. MES7 is growing
389 microaerobically in the MES, using oxygen as the terminal electron acceptor. This
390 supports the hypothesis that microaerophilic bacteria provide a supportive role to the
391 rest of the community by scrubbing low levels of oxygen that diffuse from the anode
392 chamber.
393
394 *Desulfovibrio* str. MES5 was the 3rd most abundant taxon, and likely converts CO_2 to
395 formate and while using cytochromes, formate dehydrogenase, and/or hydrogenases to
396 accept electrons from the cathode. The high expression of formate dehydrogenase (3-
397 fold, dsv-h.peg.194) and cytochromes (6-fold, dsv-h.peg.1195; 6-fold, dsv-h.peg.3868)
398 on the electrode compared to the supernatant supports this hypothesis. The lack of a
399 suitable terminal electron acceptor indicates that *Desulfovibrio* str. MES5 reduces
400 protons and generates hydrogen gas (Carepo *et al.*, 2002), which is supported by the
401 comparatively high expression of hydrogenases (dsv-h.peg.740-1) on the electrode
402 surface (>3-fold CCc vs. CCs). Furthermore, *Desulfovibrio* spp. have been shown to
403 interact with a cathode to facilitate electrohydrogenesis.\ (Aulenta *et al.*, 2012; Croese *et*
404 *al.*, 2011; Yu *et al.*, 2011). It is likely that small amounts of acetate from *Acetobacterium*
405 str. MES1 are used as a supplementary carbon source for *Desulfovibrio* str. *MES5*, but
406 based on the high hydrogenase and low acetate kinase expression pattern the majority
407 of reducing potential comes from the electrode.
408
409 While *Acetobacterium* str. MES1, *Sulfurospirillum* str. MES7, and *Desulfovibrio* str.
410 MES5 can explain most of the activity occurring in the microbial electrosynthesis
411 systems, the remaining genomes have broad metabolic capabilities, but are typically in
412 lower abundance (<7%). We hypothesize that they are consuming detritus, degradation
413 products, and/or short chain fatty acids generated by the abundant organisms. A pan-

414 genome associated with the Rhodobacteraceae family had an expression profile
415 consistent with acetate oxidation and *cbb3*-type cytochrome c oxidases that could be
416 indicative of microaerobic growth. The latter have been expressed in *Rhodobacter* sp.
417 growing in microaerobic and anaerobic conditions (Kaplan *et al.*, 2005) and were also
418 found to be upregulated by *Shewanella* oneidensis MR-1 growing on electrodes
419 (Rosenbaum *et al.*, 2012). While we are hypothesizing that these cytochrome c oxidases
420 in Rhodobacteraceae str. MES12 and *Sulfurospirillum* str. MES7 are involved in
421 microaerobic growth, given their prominence in this study and others involving
422 bioelectrochemical systems (Rosenbaum *et al.*, 2012), their role in EET should be
423 investigated further. One of two *Bacteroides* genomes (str. MES10) was closely related
424 (93% sequence identity) to *Proteiniphilum acetatigenes*, which has been shown to
425 generate acetate when growing on wastewater cell debris(Chen, 2005) and Croese et al.
426 discovered a relatively high abundance of uncultured *Bacteroides* in a hydrogen
427 producing biocathode community (Croese *et al.*, 2013), suggesting possible productive
428 roles for the *Bacteroides* str. MES9 and MES10 in the electrosynthetic microbiome.
429 Interestingly, *Bacteroides* str. MES9 expresses a butanol dehydrogenase (bacteroid-
430 h.peg.1751) on the electrode surface, which suggests that changing the operating
431 conditions of the MES could produce biofuels and other valuable products (see
432 Bioprospecting section in supporting materials). Additionally, both *Bacteroides* genomes
433 and the Sphaerochaeta str. MES8 genome exhibited high expression of ferredoxin
434 genes (bacteroid-h.peg.3284, bacteroid-l.peg.2157, sphaer.peg.2014), which may be
435 used to shuttle electrons for community metabolism.
436
437 **Metabolic model reconstructions and analysis**
438 Genome-scale metabolic models were constructed for the three dominate species in the
439 electrosynthetic community (see methods): *Acetobacterium* str. MES1, *Sulfurospirillum*

str. MES7, and *Desulfovibrio* str. MES5. These models were then used, in combination with flux balance analysis (Orth *et al.*, 2010), to predict the metabolic activity of each of these species during microbial community growth on the electrode. The accuracy of these flux predictions was evaluated by calculating the fraction of active reactions predicted by the models that were associated with actively expressed genes, as determined from the metatranscriptomic data (Table 1 and methods). In this analysis, the *Acetobacterium* model displayed only one plausible flux profile, which involved carbon fixation and acetate production via the Wood-Ljungdahl pathway using hydrogen, raw electrons, or similar reducing equivalents as an electron source. With this flux profile, there were 338 active reactions with associated genes in *Acetobacterium*, and for 258 (76%) of these reactions, at least one of the associated genes was actively expressed. Most active reactions that lacked expression support were involved in either amino acid biosynthesis or nucleotide metabolisms. The *Sulfurospirillum* model predicted two alternative theories for the metabolic role of this species: (i) reduction of CO_2 through the reductive TCA cycle with hydrogen used as the reducing agent (67% of active reactions associated with at least one expressed gene), and (ii) oxidation of acetate coupled to O_2 reduction (66% of active reactions associated with at least one expressed gene). Given the nearly equal agreement of both of these operating with our transcriptome data, and given the high abundance of *Sulfurospirillum* in our community, it is possible *Sulfurospirillum* actually performs both roles depending on its context and environment. The *Desulfovibrio* model also predicted two alternative theories for the metabolic role of this species in our electrosynthetic microbiome: (i) conversion of CO_2 and electrons/hydrogen to formate (75.7% of active reactions associated with at least one expressed gene), or (ii) consumption of acetate (75.9% of active reactions associated with at least one expressed gene). As with *Sulfurospirillum,* the expression

data was equally supportive of both metabolic theories, indicating that *Desulfovibrio* also performs a combination of carbon-fixation and acetate utilization.

In addition to evaluating the overall evidence supporting each of our predicted flux profiles, the transcriptome data was also applied to evaluate the flux profiles on a pathway-by-pathway basis, enabling a better understanding of model accuracy, and revealing insights into potential interspecies interactions (see Methods and Figure 4). Generally, this analysis showed a large degree of agreement between predicted flux profiles and expression data, with some notable exceptions: (i) the terpenoid pathways in all our models were gap-filled because the models all include ubiquinone as a component of biomass, but there is little evidence for these pathways in our genomes and it is likely these genomes are functioning anaerobically and do not have to produce ubiquinone; (ii) the *Acetobacterium* and *Desulfovibrio* models both appear to overuse their pentose-phosphate-pathways compared to what would be expected based on expression data; (iii) the *Desulfovibrio* model overuses its thiamin pathway and should actually obtain thiamin from an external source according to expression data; (iv) the *Sulfurospirillum* model overuses its sulfur and nitrogen metabolism pathways; and (v) all three models appear to underutilize the vitamin B6 and fructose and mannose metabolism pathways.

The pathway-based model analysis (Figure 4) reveals interactions and dependencies among the top genomes. *Desulfovibrio* appears to require an external source of histidine, thiamin, riboflavin, and folate, while the other genomes could be sources of all four of these compounds due to depletion or absence in the supplied medium. *Acetobacterium* appears to be unique in making glutathione, and also has far more representation in carbon fixation than the other genomes. In contrast, *Sulfurospirillum*

491 appears unique in possessing an active glyoxylate metabolism and the most active TCA
492 cycle. It is interesting to note that all three genomes appear to produce most of their own
493 amino acids, vitamins, and nucleotides, with *Desulfovibrio* being the least prototrophic of
494 the three. Biochemical reaction equations, compounds, associated flux values, and
495 comparative genomics tools including hypothetical gene knockout experiments for all the
496 models can be found at the KBase Narrative Interface:
497 https://narrative.kbase.us/narrative/ws.15248.obj.1.
498
499 **Discussion**
500 Metabolic analysis and modeling of this unique microbial community capable of
501 converting CO_2 into volatile fatty acid provides a detailed look into how communities
502 actively metabolize on an electrosynthetic biocathode. The genome-wide metabolic
503 capabilities of microorganisms in the community were determined, and a putative
504 metabolic model of the primary community members has been summarized (Figure 5).
505 CO_2 fixation and the carbon flux through the electrosynthetic microbiome center on the
506 Wood-Ljungdahl pathway of the *Acetobacterium* genome, components of which were
507 more active on the closed circuit electrode compared to any other condition tested,
508 demonstrating the importance of electrode-associated growth by *Acetobacterium*. In
509 addition, reducing equivalents in the form of hydrogen and reduced enzymes (eg.
510 ferredoxin) also stem from the *Acetobacterium,* alongside major contributions from
511 *Desulfovibrio* and *Sulfurospirillum*. Other organisms in the community are contributing to
512 overall fitness by scrubbing toxic compounds (e.g. oxygen) and providing nutrient
513 exchange. Given the proper conditions and applied drivers, this electrosynthetic
514 microbial community has a wide range of biotechnological potential, including the
515 production of alcohols, 2,3-butanediol, and polyhydroxyalkonoates (see supplementary
516 note on bioprospecting and Supplementary Table 4 for more detailed information).

Generally, the proposed mechanisms for cathodic electron transfer in the absence of added mediators are analogous to anodic electron transfer, namely that cytochromes are the primary conduit of electrons to and from the microbial cell (Holmes *et al.*, 2006; Leang *et al.*, 2010; Ross *et al.*, 2011; Inoue *et al.*, 2011; Carlson *et al.*, 2012). The role of cytochromes on anodes has been primarily elucidated in pure culture, but metatranscriptomic studies also point to cytochrome involvement in EET to anodes (Ishii *et al.*, 2013, 2015) and even less is known about EET in communities grown on cathodes. In this study, *Desulfovibrio* str. MES5 has three upregulated cytochromes on the electrode compared to the supernatant: two with a 6-fold increase (dsv-h.peg.1195 and dsv-h.peg.3868) and one with a 2.5-fold increase (dsv-h.peg.1225). The latter two were upregulated greater than 2-fold on the closed circuit cathode compared to the open circuit cathode. Additionally, a formate dehydrogenase from *Desulfovibrio* str. MES5 (dsv-h.peg.194) was upregulated nearly 3-fold on the electrode compared to supernatant, >2-fold CCc versus OCc, and could explain formate transiently observed in the supernatant (Supplementary Figure 3) (Marshall *et al.*, 2013)(da Silva *et al.*, 2013). In addition to their involvement in electron transfer at cathode surfaces, cytochromes can also act as natural mediators for hydrogenases (Pereira *et al.*, 1998; Yahata *et al.*, 2006) and could shuttle electrons from the electrode or from electrode-attached hydrogenases to the microbial community. Three NiFe hydrogenases were highly expressed by *Desulfovibrio* str. MES5 on the electrode compared to the supernatant (dsv-h.peg.740-741, >3-fold and 6-fold increase on electrode compared [CCc] to supernatant [CCs]; and dsv-h.peg.1193, 6-fold increase on electrode [CCc] compared to supernatant [CCs]). One of the NiFe hydrogenases (dsv-h.peg.1193) was adjacent to the upregulated high molecular weight cytochrome c (dsv-h.peg.1195). Given the high expression on the cathode compared to supernatant, it is hypothesized that cytochromes, hydrogenases,

543 and possibly formate dehydrogenases associated with *Desulfovibrio* str. MES5 act as
544 electron mediators between the electrode and the cell to deliver reducing equivalents. In
545 addition to the well-established role of cell-bound cytochromes in direct electron
546 transport with an electrode (Bond *et al.*, 2012; Pirbadian *et al.*, 2014), free cytochromes
547 have been shown to be integral to anodic electron transfer while still imbedded in the
548 biofilm matrix, and could be assisting electron transport to the community in this
549 electrosynthetic biofilm (Inoue *et al.*, 2011).
550
551 The recent discovery that extracellular enzymes (likely hydrogenases and formate
552 dehydrogenases) may be present in cathodic biofilms and may catalyze electron transfer
553 into microbially-utilizable substrates (hydrogen and formate) adds a new and important
554 piece to solve the EET mechanistic puzzle (Deutzmann *et al.*, 2015). Of the genes highly
555 expressed on the electrode, several redox-active electron carriers (particularly
556 hydrogenases and ferredoxins) had high differential expression on the poised electrode
557 compared to the supernatant and open circuit electrode. A *Sulfurospirillum* str. MES7
558 ferredoxin (sulfuro.peg.2444) is >2-fold higher on the electrode compared to the
559 supernatant (1.5x higher CCc vs. OCc) and the low abundance *Bacteroides str.* MES10
560 contains a ferredoxin (bacteroid-l.peg.2157) that is >9-fold upregulated on the electrode
561 compared to supernatant (1.7x higher CCc vs. OCc). Importantly, a ferredoxin from
562 *Acetobacterium* str. MES1 (aceto.peg.1713) was 7-fold higher on the electrode (CCc)
563 compared to both supernatant conditions (CCs and OCs). Additionally, the highly
564 expressed *Acetobacterium* str. MES1 hydrogenase gene cluster, *hydABCDE*
565 (aceto.peg.4025-4029), had >5-fold higher expression per cell on the electrode
566 compared to the supernatant (1.6x higher CCc vs. OCc), despite the presence of
567 hydrogen in the supernatant. The combination of soluble hydrogenases and ferredoxins
568 on the cathode could facilitate cathodic electron transfer into organisms like

569 *Acetobacterium* that contain no cytochromes and no obvious means of electron transfer
570 through the cell envelope.
571
572 Despite the lack of a redox-active signal in cell-free cyclic voltammograms and a
573 catalytic wave characteristic of direct electron transfer in the electrosynthetic microbial
574 community (Marshall *et al.*, 2013), SEM-EDX images show extracellular material with
575 elemental signatures of common redox-active enzymes (Supplementary Figure 5).
576 Additionally, no reduction in current or shift in the voltammetric peaks were observed
577 when the supernatant was replaced with fresh medium, suggesting tightly bound
578 electron transfer mechanisms. The discovery of metals such as iron and nickel on the
579 electrode surface could be concentrated enzymes, but microbial or pH induced
580 precipitation of the metals as (hydr)oxides, sulfides, carbonates, phosphates, perhaps
581 even as nanoparticles cannot be ruled out. The latter has been hypothesized by Jourdin
582 et al. who observed copper concentrated on the surface of a microbial electroacetogenic
583 cathode (Jourdin *et al.*, 2016).
584
585 Based on the highly expressed redox active proteins on the electrode (all of the proteins
586 mentioned above are in the top 5% of total genes expressed on the electrode), and the
587 consistent hydrogen production in the reactors (Marshall *et al.*, 2012, 2013; LaBelle *et*
588 *al.*, 2014), extracellular enzymes and/or concentrated metals are likely functionalizing
589 the electrode while hydrogen, ferredoxins, and/or cytochromes act as shuttles for
590 different organisms in the biofilm. This would explain why microbes lacking an outer
591 membrane can thrive on an electrode, and why previous studies ran electrohydrogenic
592 biocathodes that could sustain hydrogen generation in the absence of a carbon source
593 for over 1000 hours (Rozendal *et al.*, 2008). Further studies are underway to fully
594 characterize functionalization of electrodes by microbes so as to optimize this strategy.

595

596 The modeling results demonstrate how metabolic models are useful for interpreting
597 expression data in order to predict the role of individual species participating within a
598 mixed microbial community. The model predictions: (i) confirmed the role of
599 *Acetobacterium* as the primary species utilizing electrons to reduce CO2; (ii) identified
600 the more complex behavior of *Sulfurospirillum* as both reducing CO2 and utilizing
601 acetate; and (iii) provided more depth and detail into our understanding of the
602 heterotrophic growth of *Desulfovibrio*. These models refined models should prove to be
603 a resource for ongoing efforts to understand, and ultimately design and refine
604 electrosynthetic microbiomes.

605

606 We have provided insights into the genetic basis of electrosynthetic microbial
607 communities, which can be used for the optimization of microbial electrosynthesis
608 through operational changes and eventual pathway engineering. Furthermore, it was
609 demonstrated that a diverse set of microorganisms could be active in limited niche space
610 with carbon dioxide as the only carbon source and the electrode as the only electron
611 donor. The discovery that predominant members of the community provide an
612 ecosystem service by scrubbing oxygen makes this, and similar, electrosynthetic
613 microbial communities valuable for practical application. If deployed in true carbon-
614 capture situations such as power plants or industrial exhaust lines, oxygen scrubbing to
615 protect the electrosynthetic anaerobes will be important. Finally, the comprehensive
616 analysis of the genomes and development of metabolic models provide the framework to
617 boost production rates and elevate this system to a platform chemical synthesis
618 technology.

619

620 **Acknowledgements**

We thank Drew Latta for SEM-EDX work and Fangfang Xia and Sebastien Boisvert for initial metagenome assembly advice. C.W.M. was supported in part by an Argonne National Laboratory Director's Fellowship. The project was funded by the Department of Energy, Advanced Projects Research Agency – Energy (DE-AR0000089) and Office of Naval Research: Grant# N00014-15-1-2219. We also acknowledge the University of Chicago Research Computing Center for their support.

Conflict of Interest

The authors declare no competing financial interests.

References

Albertsen M, Hugenholtz P, Skarshewski A, Nielsen KL, Tyson GW, Nielsen PH. (2013). Genome sequences of rare, uncultured bacteria obtained by differential coverage binning of multiple metagenomes. *Nat Biotechnol* **31**: 533–538.

Aulenta F, Catapano L, Snip L, Villano M, Majone M. (2012). Linking Bacterial Metabolism to Graphite Cathodes: Electrochemical Insights into the H2-Producing Capability of Desulfovibrio sp. *ChemSusChem* **5**: 1080–1085.

Aziz RK, Bartels D, Best AA, DeJongh M, Disz T, Edwards RA, *et al.* (2008). The RAST Server: Rapid Annotations using Subsystems Technology. *BMC Genomics* **9**: 75.

Bankevich A, Nurk S, Antipov D, Gurevich AA, Dvorkin M, Kulikov AS, *et al.* (2012). SPAdes: A New Genome Assembly Algorithm and Its Applications to Single-Cell Sequencing. *J Comput Biol* **19**: 455–477.

Boisvert S, Raymond F, Godzaridis É, Laviolette F, Corbeil J. (2012). Ray Meta: scalable de novo metagenome assembly and profiling. *Genome Biol* **13**: R122.

Bond DR, Strycharz-Glaven SM, Tender LM, Torres CI. (2012). On Electron Transport through Geobacter Biofilms. *ChemSusChem* **5**: 1099–1105.

Brettin T, Davis JJ, Disz T, Edwards RA, Gerdes S, Olsen GJ, *et al.* (2015). RASTtk: A modular and extensible implementation of the RAST algorithm for building custom annotation pipelines and annotating batches of genomes. *Sci Rep* **5**. e-pub ahead of print, doi: 10.1038/srep08365.

Bruant G, Lévesque M-J, Peter C, Guiot SR, Masson L. (2010). Genomic Analysis of Carbon Monoxide Utilization and Butanol Production by Clostridium carboxidivorans Strain P7T. *PLoS ONE* **5**: e13033.

Camacho C, Coulouris G, Avagyan V, Ma N, Papadopoulos J, Bealer K, *et al.* (2009). BLAST+: architecture and applications. *BMC Bioinformatics* **10**: 421.

Carepo M, Baptista JF, Pamplona A, Fauque G, Moura JJG, Reis MAM. (2002). Hydrogen metabolism in Desulfovibrio desulfuricans strain New Jersey (NCIMB

659 8313)—comparative study with D. vulgaris and D. gigas species. *Anaerobe* **8**: 325–
660 332.

661 Carlson HK, Iavarone AT, Gorur A, Yeo BS, Tran R, Melnyk RA, *et al.* (2012). Surface
662 multiheme c-type cytochromes from Thermincola potens and implications for
663 respiratory metal reduction by Gram-positive bacteria. *Proc Natl Acad Sci* **109**:
664 1702–1707.

665 Chen S. (2005). Proteiniphilum acetatigenes gen. nov., sp. nov., from a UASB reactor
666 treating brewery wastewater. *Int J Syst Evol Microbiol* **55**: 2257–2261.

667 Cheng S, Xing D, Call DF, Logan BE. (2009). Direct Biological Conversion of Electrical
668 Current into Methane by Electromethanogenesis. *Environ Sci Technol* **43**: 3953–
669 3958.

670 Croese E, Keesman KJ, Widjaja-Greefkes (Aura) H. C. A., Geelhoed JS, Plugge CM,
671 Sleutels THJA, *et al.* (2013). Relating MEC population dynamics to anode
672 performance from DGGE and electrical data. *Syst Appl Microbiol* **36**: 408–416.

673 Croese E, Pereira MA, Euverink G-JW, Stams AJM, Geelhoed JS. (2011). Analysis of
674 the microbial community of the biocathode of a hydrogen-producing microbial
675 electrolysis cell. *Appl Microbiol Biotechnol* **92**: 1083–1093.

676 Curatti L, Brown CS, Ludden PW, Rubio LM. (2005). Genes required for rapid
677 expression of nitrogenase activity in Azotobacter vinelandii. *Proc Natl Acad Sci U S A*
678 **102**: 6291–6296.

679 Deutzmann JS, Sahin M, Spormann AM. (2015). Extracellular Enzymes Facilitate
680 Electron Uptake in Biocorrosion and Bioelectrosynthesis. *mBio* **6**: e00496-15.

681 Dick GJ, Andersson AF, Baker BJ, Simmons SL, Thomas BC, Yelton AP, *et al.* (2009).
682 Community-wide analysis of microbial genome sequence signatures. *Genome Biol*
683 **10**: R85.

684 Dreyfuss JM, Zucker JD, Hood HM, Ocasio LR, Sachs MS, Galagan JE. (2013).
685 Reconstruction and validation of a genome-scale metabolic model for the
686 filamentous fungus Neurospora crassa using FARM. *PLoS Comput Biol* **9**: e1003126.

687 Edgar RC. (2010). Search and clustering orders of magnitude faster than BLAST.
688 *Bioinformatics* **26**: 2460–2461.

689 Goris T, Schubert T, Gadkari J, Wubet T, Tarkka M, Buscot F, *et al.* (2014). Insights
690 into organohalide respiration and the versatile catabolism of Sulfurospirillum
691 multivorans gained from comparative genomics and physiological studies. *Environ*
692 *Microbiol* **16**: 3562–3580.

693 Henry CS, DeJongh M, Best AA, Frybarger PM, Linsay B, Stevens RL. (2010). High-
694 throughput generation, optimization and analysis of genome-scale metabolic
695 models. *Nat Biotechnol* **28**: 977–982.

696 Henry CS, Jankowski MD, Broadbelt LJ, Hatzimanikatis V. (2006). Genome-scale
697 thermodynamic analysis of Escherichia coli metabolism. *Biophys J* **90**: 1453–1461.

698 Henry CS, Zinner JF, Cohoon MP, Stevens RL. (2009). iBsu1103: a new genome-scale
699 metabolic model of Bacillus subtilis based on SEED annotations. *Genome Biol* **10**:
700 R69.

701 Holmes DE, Chaudhuri SK, Nevin KP, Mehta T, Methé BA, Liu A, *et al.* (2006).
702 Microarray and genetic analysis of electron transfer to electrodes in Geobacter
703 sulfurreducens. *Environ Microbiol* **8**: 1805–1815.

704 Hügler M, Wirsen CO, Fuchs G, Taylor CD, Sievert SM. (2005). Evidence for
705 Autotrophic CO2 Fixation via the Reductive Tricarboxylic Acid Cycle by Members of
706 the ε Subdivision of Proteobacteria. *J Bacteriol* **187**: 3020–3027.

707 Hyatt D, Chen G-L, LoCascio PF, Land ML, Larimer FW, Hauser LJ. (2010). Prodigal:
708 prokaryotic gene recognition and translation initiation site identification. *BMC*
709 *Bioinformatics* **11**: 119.

710 Inoue K, Leang C, Franks AE, Woodard TL, Nevin KP, Lovley DR. (2011). Specific
711 localization of the c-type cytochrome OmcZ at the anode surface in current-
712 producing biofilms of Geobacter sulfurreducens. *Environ Microbiol Rep* **3**: 211–217.

713 Ishii S, Suzuki S, Norden-Krichmar TM, Tenney A, Chain PSG, Scholz MB, *et al.*
714 (2013). A novel metatranscriptomic approach to identify gene expression dynamics
715 during extracellular electron transfer. *Nat Commun* **4**: 1601.

716 Ishii S, Suzuki S, Tenney A, Norden-Krichmar TM, Nealson KH, Bretschger O. (2015).
717 Microbial metabolic networks in a complex electrogenic biofilm recovered from a
718 stimulus-induced metatranscriptomics approach. *Sci Rep* **5**. e-pub ahead of print,
719 doi: 10.1038/srep14840.

720 Jankowski MD, Henry CS, Broadbelt LJ, Hatzimanikatis V. (2008). Group contribution
721 method for thermodynamic analysis of complex metabolic networks. *Biophys J* **95**:
722 1487–1499.

723 Jeong H-S, Jouanneau Y. (2000). Enhanced Nitrogenase Activity in Strains of
724 Rhodobacter capsulatus That Overexpress the rnf Genes. *J Bacteriol* **182**: 1208–
725 1214.

726 Jourdin L, Lu Y, Flexer V, Keller J, Freguia S. (2016). Biologically Induced Hydrogen
727 Production Drives High Rate/High Efficiency Microbial Electrosynthesis of Acetate
728 from Carbon Dioxide. *ChemElectroChem* n/a-n/a.

729 Kanehisa M, Goto S. (2000). KEGG: Kyoto Encyclopedia of Genes and Genomes.
730 *Nucleic Acids Res* **28**: 27–30.

731 Kaplan S, Eraso J, Roh JH. (2005). Interacting regulatory networks in the facultative
732 photosynthetic bacterium, Rhodobacter sphaeroides 2.4.1. *Biochem Soc Trans* **33**:
733 51–55.

734 Karp PD, Riley M, Paley SM, Pellegrini-Toole A. (2002). The MetaCyc Database.
735 *Nucleic Acids Res* **30**: 59–61.

736 Kiely PD, Regan JM, Logan BE. (2011). The electric picnic: synergistic requirements
737 for exoelectrogenic microbial communities. *Curr Opin Biotechnol* **22**: 378–385.

738 LaBelle EV, Marshall CW, Gilbert JA, May HD. (2014). Influence of Acidic pH on
739 Hydrogen and Acetate Production by an Electrosynthetic Microbiome. *PLoS ONE* **9**:
740 e109935.

741 Latendresse M. (2014). Efficiently gap-filling reaction networks. *BMC Bioinformatics*
742 **15**: 225.

743 Leang C, Qian X, Mester T, Lovley DR. (2010). Alignment of the c-Type Cytochrome
744 OmcS along Pili of Geobacter sulfurreducens. *Appl Environ Microbiol* **76**: 4080–4084.

745 Lee HJ, Gennis RB, Ädelroth P. (2011). Entrance of the proton pathway in cbb3-type
746 heme-copper oxidases. *Proc Natl Acad Sci* **108**: 17661–17666.

747 Li H, Durbin R. (2009). Fast and accurate short read alignment with Burrows–
748 Wheeler transform. *Bioinformatics* **25**: 1754–1760.

749 Marshall CW, Ross DE, Fichot EB, Norman RS, May HD. (2012). Electrosynthesis of
750 Commodity Chemicals by an Autotrophic Microbial Community. *Appl Environ*
751 *Microbiol* **78**: 8412–8420.

752 Marshall CW, Ross DE, Fichot EB, Norman RS, May HD. (2013). Long-term Operation
753 of Microbial Electrosynthesis Systems Improves Acetate Production by Autotrophic
754 Microbiomes. *Environ Sci Technol* **47**: 6023–6029.

755 Meyer F, Paarmann D, D'Souza M, Olson R, Glass EM, Kubal M, *et al.* (2008). The
756 metagenomics RAST server – a public resource for the automatic phylogenetic and
757 functional analysis of metagenomes. *BMC Bioinformatics* **9**: 386.

758 Miller CS, Baker BJ, Thomas BC, Singer SW, Banfield JF. (2011). EMIRGE:
759 reconstruction of full-length ribosomal genes from microbial community short read
760 sequencing data. *Genome Biol* **12**: R44.

761 Namiki T, Hachiya T, Tanaka H, Sakakibara Y. (2012). MetaVelvet: an extension of
762 Velvet assembler to de novo metagenome assembly from short sequence reads.
763 *Nucleic Acids Res* **40**: e155–e155.

764 Nevin KP, Woodard TL, Franks AE, Summers ZM, Lovley DR. (2010). Microbial
765 Electrosynthesis: Feeding Microbes Electricity To Convert Carbon Dioxide and
766 Water to Multicarbon Extracellular Organic Compounds. *mBio* **1**: e00103-10.

767 Orth JD, Thiele I, Palsson BØ. (2010). What is flux balance analysis? *Nat Biotechnol*
768 **28**: 245–248.

769 Parks DH, Imelfort M, Skennerton CT, Hugenholtz P, Tyson GW. (2015). CheckM:
770 assessing the quality of microbial genomes recovered from isolates, single cells, and
771 metagenomes. *Genome Res* gr.186072.114.

772 Peng Y, Leung HCM, Yiu SM, Chin FYL. (2012). IDBA-UD: a de novo assembler for
773 single-cell and metagenomic sequencing data with highly uneven depth.
774 *Bioinformatics* **28**: 1420–1428.

775 Pereira IAC, Romão CV, Xavier AV, LeGall J, Teixeira M. (1998). Electron transfer
776 between hydrogenases and mono- and multiheme cytochromes in Desulfovibrio ssp.
777 *JBIC J Biol Inorg Chem* **3**: 494–498.

778 Pirbadian S, Barchinger SE, Leung KM, Byun HS, Jangir Y, Bouhenni RA, *et al.* (2014).
779 Shewanella oneidensis MR-1 nanowires are outer membrane and periplasmic
780 extensions of the extracellular electron transport components. *Proc Natl Acad Sci*
781 **111**: 12883–12888.

782 Quast C, Pruesse E, Yilmaz P, Gerken J, Schweer T, Yarza P, *et al.* (2013). The SILVA
783 ribosomal RNA gene database project: improved data processing and web-based
784 tools. *Nucleic Acids Res* **41**: D590–D596.

785 Rabaey K, Rozendal RA. (2010). Microbial electrosynthesis — revisiting the
786 electrical route for microbial production. *Nat Rev Microbiol* **8**: 706–716.

787 Rosenbaum MA, Bar HY, Beg QK, Segrè D, Booth J, Cotta MA, *et al.* (2012).
788 Transcriptional Analysis of Shewanella oneidensis MR-1 with an Electrode
789 Compared to Fe(III)Citrate or Oxygen as Terminal Electron Acceptor. *PLoS ONE* **7**:
790 e30827.

791 Ross DE, Flynn JM, Baron DB, Gralnick JA, Bond DR. (2011). Towards
792 Electrosynthesis in Shewanella: Energetics of Reversing the Mtr Pathway for
793 Reductive Metabolism. *PLoS ONE* **6**: e16649.

794 Ross DE, Marshall CW, May HD, Norman RS. (2016). Comparative Genomic Analysis
795 of Sulfurospirillum cavolei MES Reconstructed from the Metagenome of an
796 Electrosynthetic Microbiome. *PLOS ONE* **11**: e0151214.

797 Rozendal RA, Jeremiasse AW, Hamelers HVM, Buisman CJN. (2008). Hydrogen
798 Production with a Microbial Biocathode. *Environ Sci Technol* **42**: 629–634.

799 Ryu M-H, Hull NC, Gomelsky M. (2014). Metabolic engineering of Rhodobacter
800 sphaeroides for improved hydrogen production. *Int J Hydrog Energy* **39**: 6384–6390.

801 Schuchmann K, Müller V. (2014). Autotrophy at the thermodynamic limit of life: a
802 model for energy conservation in acetogenic bacteria. *Nat Rev Microbiol* **12**: 809–
803 821.

804 da Silva SM, Voordouw J, Leitao C, Martins M, Voordouw G, Pereira IAC. (2013).
805 Function of formate dehydrogenases in Desulfovibrio vulgaris Hildenborough
806 energy metabolism. *Microbiology* **159**: 1760–1769.

807 Steinbusch KJJ, Hamelers HVM, Schaap JD, Kampman C, Buisman CJN. (2010).
808 Bioelectrochemical Ethanol Production through Mediated Acetate Reduction by
809 Mixed Cultures. *Environ Sci Technol* **44**: 513–517.

810 Suzek BE, Wang Y, Huang H, McGarvey PB, Wu CH, Consortium the U. (2015).
811 UniRef clusters: a comprehensive and scalable alternative for improving sequence
812 similarity searches. *Bioinformatics* **31**: 926–932.

813 Tremblay P-L, Zhang T. (2015). Electrifying microbes for the production of
814 chemicals. *Microb Physiol Metab* 201.

815 Wang Z, Leary DH, Malanoski AP, Li RW, Hervey WJ, Eddie BJ, *et al.* (2015). A
816 Previously Uncharacterized, Nonphotosynthetic Member of the Chromatiaceae Is
817 the Primary CO2-Fixing Constituent in a Self-Regenerating Biocathode. *Appl Environ*
818 *Microbiol* **81**: 699–712.

819 Wu S, Zhu Z, Fu L, Niu B, Li W. (2011). WebMGA: a customizable web server for fast
820 metagenomic sequence analysis. *BMC Genomics* **12**: 444.

821 Yahata N, Saitoh T, Takayama Y, Ozawa K, Ogata H, Higuchi Y, *et al.* (2006). Redox
822 Interaction of Cytochrome c3 with [NiFe] Hydrogenase from Desulfovibrio vulgaris
823 Miyazaki F†. *Biochemistry (Mosc)* **45**: 1653–1662.

824 Yu L, Duan J, Zhao W, Huang Y, Hou B. (2011). Characteristics of hydrogen evolution
825 and oxidation catalyzed by Desulfovibrio caledoniensis biofilm on pyrolytic graphite
826 electrode. *Electrochimica Acta* **56**: 9041–9047.

827 Zerbino DR, Birney E. (2008). Velvet: Algorithms for de novo short read assembly
828 using de Bruijn graphs. *Genome Res* **18**: 821–829.

829
830
831
832

833 Table 1. Transcriptome support for metabolic activity predicted by models

Species	Description	Active reactions^	Supported reactions*	Expressed genes
Acetobacterium	C02 fixation to acetate	338/1244	258/338	402/954
Sulfurospirillum	Reduction of CO2	328/1143	219/328	252/661
Sulfurospirillum	Oxidation of acetate	330/1142	218/330	252/661
Desulfovibrio	Conversion of CO2 to formate	322/1124	244/322	425/759
Desulfovibrio	Consumption of acetate	320/1124	243/320	425/759

834 ^Active reactions only include reactions with associated genes (gapfilled reactions
835 filtered out)
836 *Supported reactions are active reactions (gapfilled reactions filtered out) associated
837 with at least one actively expressed gene
838

839 Figure 1. Reactor performance over time. (A) Acetate production in CC and OC – breaks
840 in plotted lines indicate an exchange of the medium, (B) acetate production rate in CC
841 and OC, and (C) accounting of the coulombs over a seven day period between medium
842 exchanges in CC and OC, numbers are percent coulombic efficiency with total percent
843 efficiency averaged over the 7 days in parentheses.

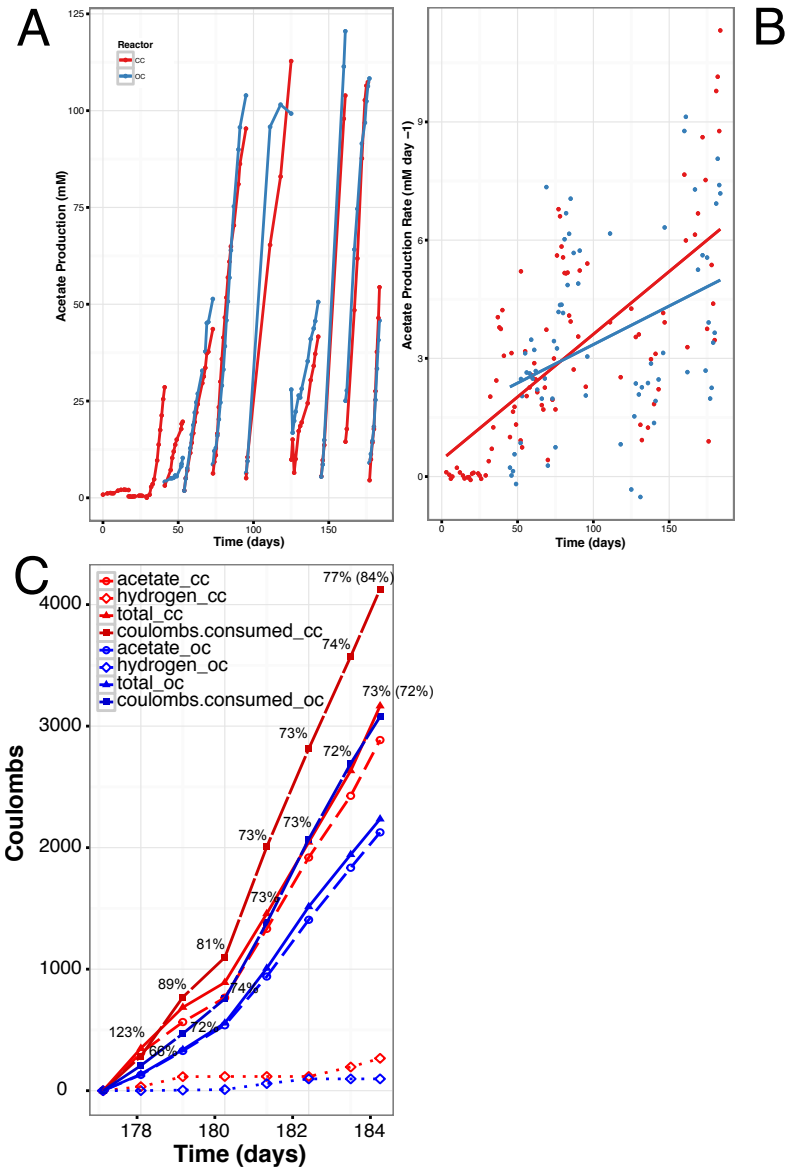

844

Figure 2. (A) Phylogenetic tree of the CCc microbial community using EMIRGE-based reconstructed 16S rRNA gene sequences (blue) and relative abundance values in parentheses and indicated by the relative size of the blue circle. Sequences were aligned using MUSCLE and the evolutionary history was inferred using the Maximum Likelihood method based on the Jukes-Cantor model. Bootstrapping support greater than 50% is indicated on the tree and is based on 1,000 iterations. (B) ESOM based on tetranucleotide frequency in the CC cathode metagenome.

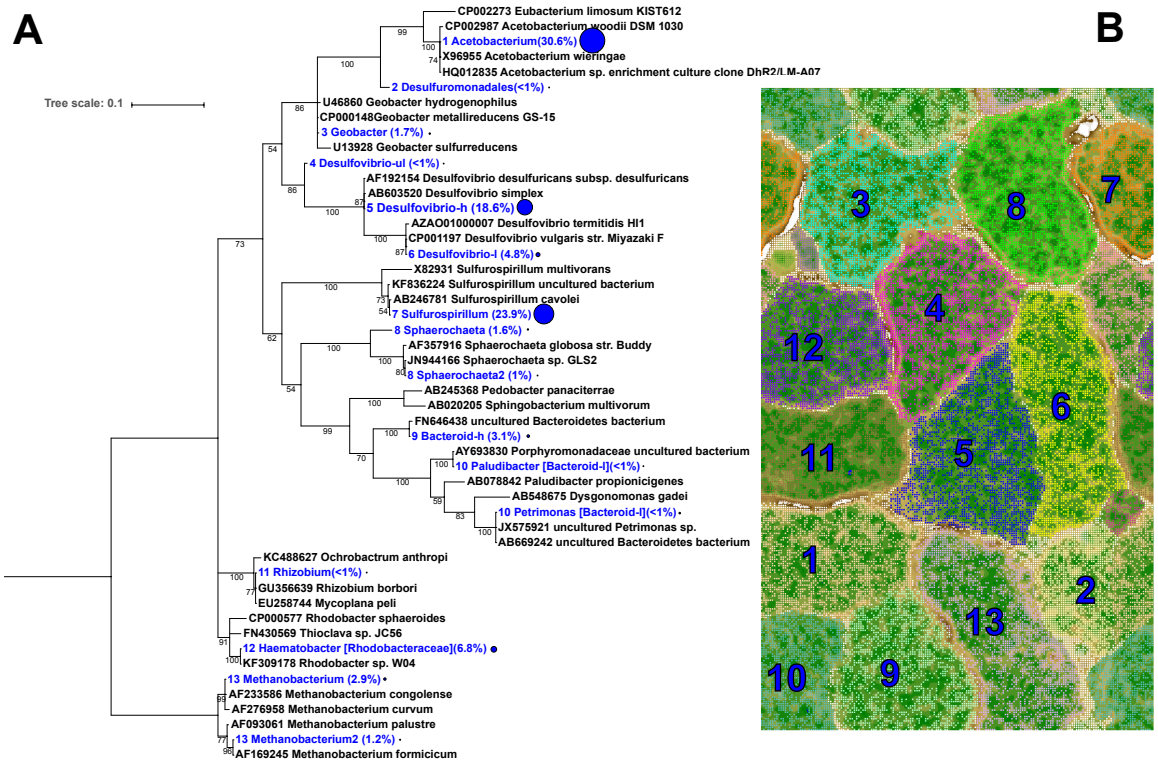

857 Figure 3. Expression profile and comparative expression of important genes. The green
858 panel shows relative expression between microorganisms and the red panel compares
859 differential expression between condition

860

Figure 4. Pathway flux and model agreement with expression data. The degree of agreement between the model-based flux predictions and expression data for each of the three metabolic models is shown, both for the entire models and broken down by categories of metabolism. In the graph, reactions are divided into five categories based on their flux and the expression of their associated genes: (i) reactions that are active and associated with at least one expressed gene (dark blue); (ii) reactions that are inactive and associated only with unexpressed genes (dark red); (iii) reactions that are inactive and associated with one or more expressed genes (green); (iv) reactions that are active and associated only with unexpressed genes (purple); and (v) gapfilled reactions associated with no genes. The dark blue and dark red categories indicate agreement between the models and expression data; purple and green categories indicate disagreement.

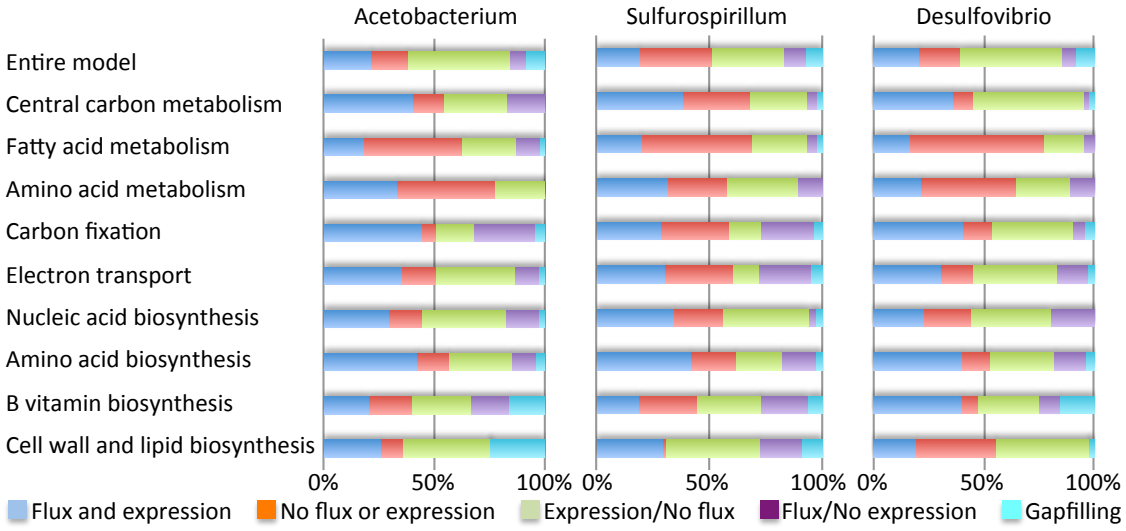

874 Figure 5. Hypothetical model of key metabolic activities and interactions among
875 dominant members of the electrosynthetic microbial community.

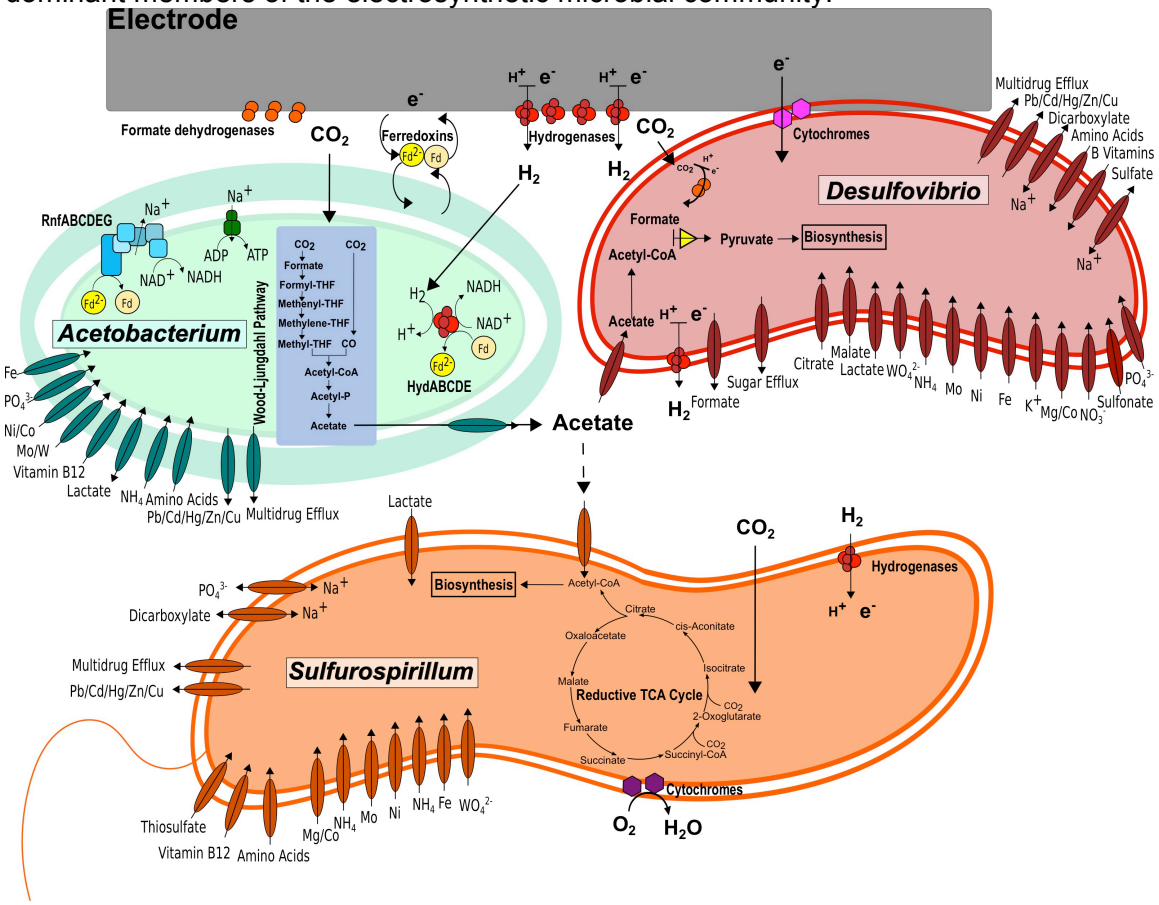

876
877
878
879
880
881
882
883
884
885
886
887